Available online at www.sciencedirect.com
ScienceDirect
Ceramics International 37 (2011) 2151–2157
CERAMICS INTERNATIONAL
www.elsevier.com/locate/ceramint

# Synthesis and properties of ceramic-based nanocomposite layer of aluminum carbide embedded with oriented carbon nanotubes

M. Aliofkhazraei [a,*], Mohammad Yousefi [b], Sh. Ahangarani [c], A. Sabour Rouhaghdam [a,*]

[a] Department of Materials Science, Faculty of Engineering, Tarbiat Modares University, Tehran, Iran, P.O.Box: 14115-143
[b] X-ray laboratory, Faculty of Science, Tarbiat Modares University, Tehran, Iran, Posatal code: 1411713116
[c] Department of Advanced Materials and Renewable Energies, Iranian Research Organization for Science and Technology (IROST), P.O. Box 15815-3538, Tehran, Iran

Received 14 December 2010; received in revised form 30 January 2011; accepted 1 March 2011
Available online 8 April 2011

**Abstract**

In the present work, carbon nanotubes (CNTs) were embedded in aluminum carbide coating in desired vertical/horizontal direction in order to fabricate a nanocomposite layer with unidirectional enhanced mechanical properties. A novel method based on monopolar pulsed plasma electrolysis under magnetic field was used for this purpose. Nanostructure of the obtained nanocomposite layer was examined with high precision figure analysis of SEM, AFM and TEM nanostructures. The mechanical and tribological properties of these coatings were investigated with respect to the direction of the embedded CNTs. The coefficient of friction was lowered from 0.2 to less than 0.1 in a pin-on-disc test against steel with dramatic affected coating wear rate by a decrease to near 400% with respect to raw substrate. The lower friction is attributed to more extensive creation of amorphous carbon on the counter surface and also in the coating wear track. As a conclusion, this method is appropriate for fabrication of hard coating on the surface of low-melting-point metals and light alloys.


*Keywords:* A. Films; B. Nanocomposites; C. Wear resistance; D. Carbides

## 1. Introduction

The composite plasma electrolysis (CPE) technique is a low-cost method suitable for fabrication of ceramic-based matrix composite coatings for such purposes as corrosion and abrasion resistance [1–4]. These coatings can contain hard particles such as WC, $Al_2O_3$ and $ZrO_2$ in a deposited matrix such as titania or titanium carbide. Recently, production of reinforcing hard powders with decreasing sizes has found industrial interest to fabricate new composites with better properties by applying of micro- and especially nanoparticles [5–7]. The term ''size effect'' for nanoparticles can describe the leading role of these nanocomposites [8]. Researchers have shown that nanocomposite coatings usually reveal enhanced mechanical, electrochemical and thermal properties as compared to pure ceramic coatings as well as microcomposite coatings [9]. The improvement of these characteristics depends mainly on the size, distribution and the amount of the embedded nanoparticles in the matrix [10–12].

One of these nanoparticles that has recently attracted the attention of many researchers for fabrication of nanocomposite coatings, is carbon nanotube (CNT). Carbon nanotubes have specific mechanical properties, which came from their unique structure (huge length to diameter ratio) [13–15]. They have recently been fabricated ceramic, metallic and polymeric based nanocomposite coatings. As these nanoparticles have different mechanical properties on their different orientations, some researchers have tried to fabricate nanocomposite coatings using oriented CNTs [16,17]. Also these materials have self-lubrication properties.

In the case of mechanical properties, however, the friction and wear resistance of nanocomposite coatings, modified by embedding some hard nanoparticles [18–20] but application of self-lubricant and oriented nanocomposite coatings can be of interest, especially for ceramic based nanocomposite coatings, which seems to have been studied less than other types of nanocomposite coatings. So in the present work, our main

* Corresponding authors. Tel.: +98 912 6905626; fax: +98 21 66960664.
*E-mail addresses:* maliofkh@gmail.com, khazrayie@modares.ac.ir (M. Aliofkhazraei), sabour@modares.ac.ir, sabour01@gmail.com (A.S. Rouhaghdam).

0272-8842/$36.00 
doi:10.1016/j.ceramint.2011.03.057

attempt was to fabricate of aluminum carbide matrix nanocomposite coatings containing carbon nanotubes (CNT) with an average diameter of 54 nm. The friction and wear performance of the fabricated coatings were analyzed in accordance to the direction of the embedded carbon nanotubes. Based on some empirical results and the mechanism of coating process, a model was developed for deposition of these kinds of coatings.

## 2. Experimental

Coin shaped (20 mm Ø × 2 mm) samples were machined from a 6082 aluminum alloy bar. The surfaces of samples were mechanically abraded by SiC paper (80 to 3000 #) and then polished on the surface of a soft cloth with the addition of appropriate abrasive solution. The preparation method and coating process are similar to our previous work [21]. In this study, multi-wall carbon nanotubes (MWCNTs) (received from Plasma Chem Company – Germany) were added to the electrolyte (10 $g.l^{-1}$). Figure 1 illustrates the SEM micro-structure of the used CNTs. The average diameter of the CNTs was equal to 54 nm, which was calculated by the figure analysis of different SEM nanostructures and is not the reported data by its manufacturer. The electrolyte went under ultra sonic condition before usage for coating process. High magnetic fields were used in two modes for arranging the conductive nanoparticles in two directions with respect to the free surface of the substrate [16,22]. So, two kinds of nanocomposite layers were fabricated: Vertical oriented nanocomposite (VON) and horizontal oriented nanocomposite (HON). In order to measure the embedded CNTs in the nanocomposite layer, the weight of the used CNTs was measured before and after the coating process and ultra precision was applied for drying the electrolyte and collecting the nanoparticles. The coatings were characterized by scanning electro microscope (SEM, Philips XL-30), atomic force microscope (AFM, NanoScope II) and transmission electron microscope (TEM, CM-200 FEG Philips). Wear tests were done for the fabricated coatings according to the ASTM G-99 [23,24] pin-on-disc guidelines. WC-Co interfaces were used as pins and substrates were used as discs. Friction coefficient was monitored by this rig while mass loss data were measured by a Sartorius (CP324S) micro-balance. This micro-balance was also used for measuring the weight of the used CNTs before and after the coating process. The mechanical and tribological properties of these coatings were investigated with respect to the direction of the embedded nanoparticles. Some of the tests were done more than twice for ensuring the achieved data.

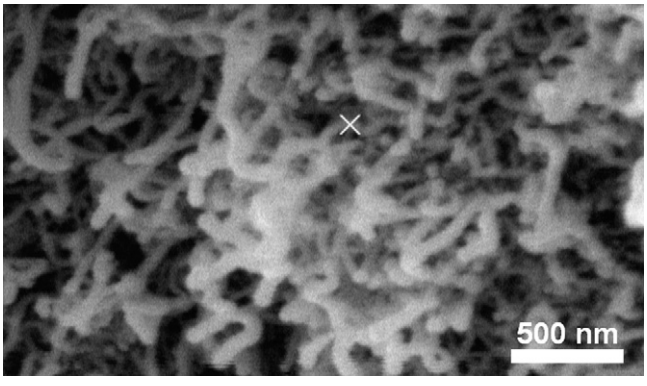


Figure 1. SEM microstructure of used CNT (average size 54 nm, indicated CNT has a diameter of 44 nm).

## 3. Results and discussion

### 3.1. Coating thickness, roughness and hardness

Figure 2 shows the variation of coating thickness with processing time for both of the fabricated nanocomposite layers. In plasma electrolytic saturation (PES) treatment, coating thickness will increase linearly with respect to the second root of the treatment time [25]. Though in some investigations, a linear increase has been reported for coating thickness, but it seems that in these papers long treatment times have not been studied [26]. Long coating times caused coating thickness to increase and hence the density of discharges became lower and lower. VON fabricated layers have lower deposition rate than HON layers.

Surface roughness of the coatings increased with the increase of treatment time (Figure 3). The roughness values of VON layers were higher than HON ones. This result was predictable due to the orientation of carbon nanotubes. Figure 4 shows the variations of surface microhardness for both VON and HON layers with respect to the processing time. VON layers showed a little higher surface hardness than HON layers; however, the error bars shown in Figure 4 interfere with each other. Increasing of coating time led to continuous increasing in the surface hardness, which is probably due to the fabrication of a thicker harder layer. As the hardness of substrate is very lower than that of the hard layer, it seems that thicker layers act as a support for performing microhardness test. Thinner coatings were cracked in the hardness tests because the relative soft substrate can not support the layer during the force loading in the hardness test [27–29]. As shown in Figure 4, the values of surface microhardness are approximately constant for the coatings thicker than 15 microns (4 h of coating process).

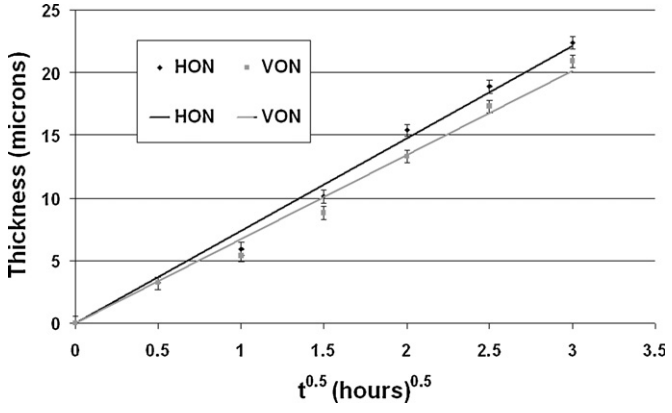


Figure 2. Variations of coating thickness with second root of processing time for both fabricated nanocomposite layers.

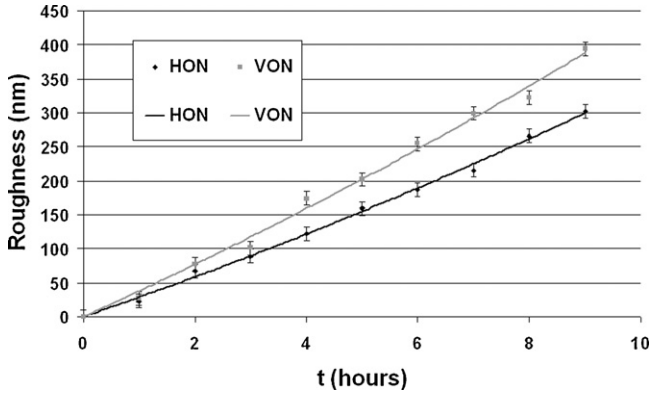


Figure 3. Variations of surface roughness with the treatment time.

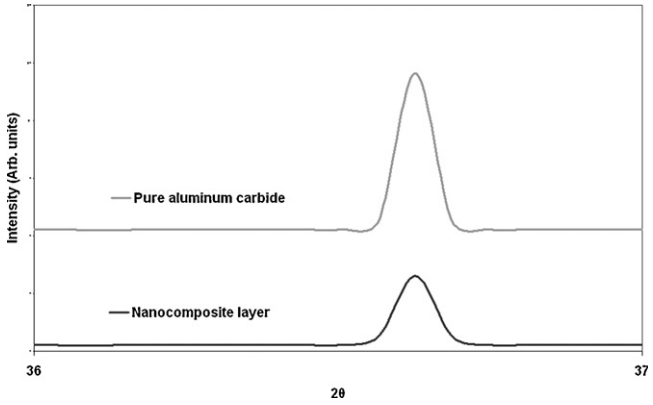


Figure 5. One x-ray diffraction peak for pure $Al_4C_3$ and nanocomposite layer.

### 3.2. Nanostructural and phase characteristics

One X-ray diffraction peak with higher width value for nanocomposite layers in comparison with pure $Al_4C_3$ is shown in Figure 5 for better illustration of the differences in full width at half maximum (FWHM). Pure aluminum carbide was analyzed in our previous paper [21]. In a good agreement with previous studies, nanoparticles decreased the average size of the grains for aluminum carbide matrix [30]. No significant difference was observed for the phase analysis of VON and HON layers. Figure 6 illustrates the SEM microstructures of the surfaces of VON and HON layers. It is notable that surface microstructure is composed of some deposited planar areas (DPAs), which are the effects of discharges over the surface. These DPAs (in the form of volcano) were also observed for PEO coatings [31–35]. VON layers seem to have more rough surfaces than HON layers, confirming the data presented in the section 3.1. Precise analysis of roughness and surface uniformity in nanoscale was performed by AFM images of the fabricated layers (Figure 7). VON layers showed more roughness than HON layers. It is notable that the sizes of DPAs are a little higher for HON than VON layers under similar conditions of coating process. Figure 8 shows the TEM nanostructures of both of the fabricated layers. Distribution of carbon nanotubes is well indicated in these figures. Although both of them were achieved in same direction during the preparation of samples but the direction of CNTs in the matrix was different. In spite of the orientation, the distribution of CNTs in nanocomposite layers was similar for both of the VON and HON layers; however, the amount of CNTs in VON layers was higher than in HON layers.

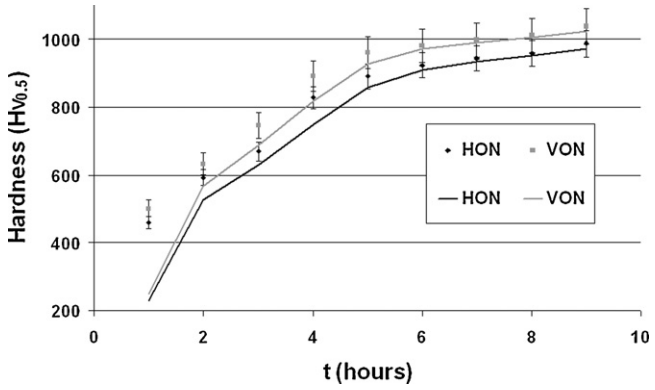


Figure 4. Variations of surface microhardness for VON and HON layers with respect to processing time.

### 3.3. Characteristics of discharges

#### 3.3.1. Size of the DPAs

Assuming (ideal status) that the DPAs have a circular shape, then their size and distribution were analyzed through different SEM microstructures. In general, their size remained approximately constant with increasing of the time of coating process, while VON layers showed lower sizes of DPAs as compared with the HON layers. The variation of DPAs average diameters

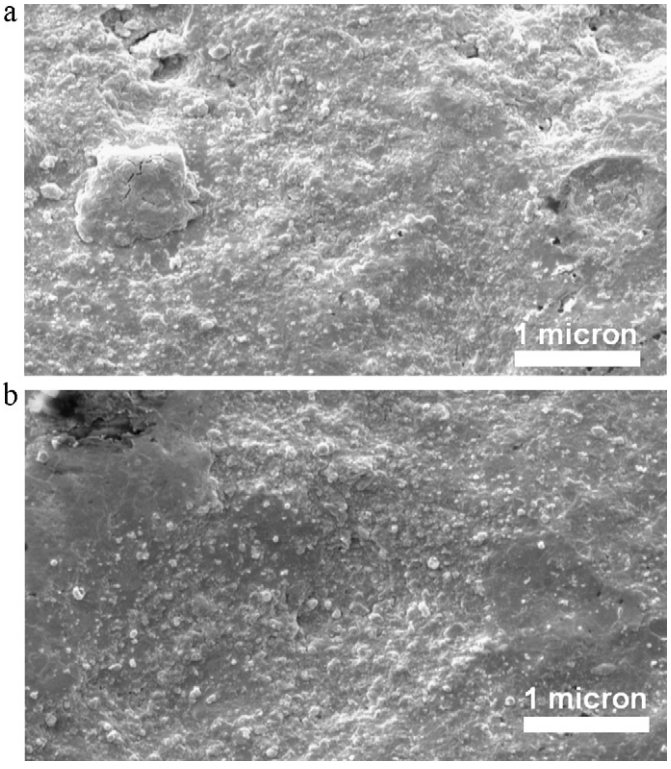


Figure 6. SEM microstructures of the surfaces of (a) VON and (b) HON layers.

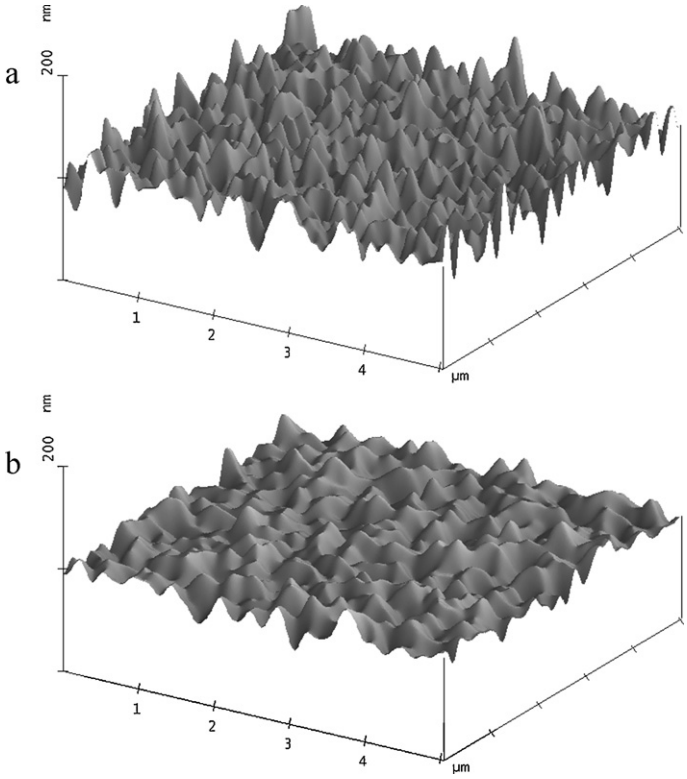


Figure 7. AFM surface images of fabricated (a) VON and (b) HON layers.

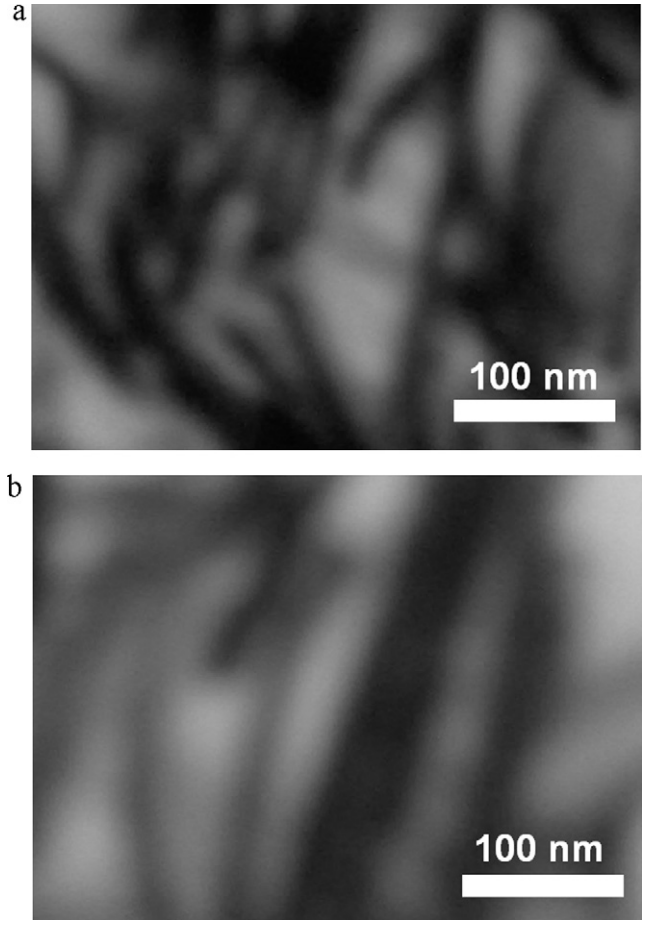


Figure 8. TEM nanostructures of fabricated (a) VON and (b) HON layers.

with respect to coating time for both layers was remained approximately unchanged at around 72 microns. In fact, the diameter of DPAs is related to the size of sparks, which is affected from the size of the gas bubbles on the surface [36]. Since the formation of gas bubbles is highly dependent on the applied voltage [37,38] and it was constant in this study, so the DPAs diameters remained approximately constant.

### 3.3.2. Density of DPAs ($N_{DPA}$)

Figure 9 illustrates the distribution of deposited areas on the surface of the sample. The number of these areas decreased with the increase of coating time (in constant applied voltage). This number was calculated by extrapolating the number of DPAs for different SEM figures. The obtained plot was in proportion with $t^{-0.5}$.

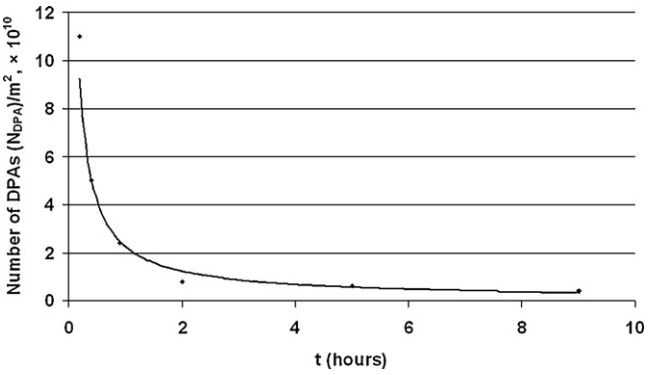


Figure 9. Number of deposited areas on the surface of the sample versus treatment time.

## 4. Mechanisms of coating formation in PES process

Formation, collapse and implode of gas bubbles on the surface of the cathode in PES treatment were well explained in the mechanism review of this process [36]. The presence of oriented CNTs in the electrolyte, their adsorption in the gas bubbles and finally their diffusion toward the surface by sparking are the differences in this study. Considering the achieved results, it can be said that collapsing plasma bubble is more suitable for vertical diffusion of the CNTs into the surface. A gas bubble has a surface force in its outer surface [39–42]. When a nanoparticle drops into the bubble, it must overcome this force. Lower surface area during the contact and also sharp edges of the nanoparticles accelerate such fallings. This phenomenon is like the contacting of a needle with a balloon. If the needle contacts from its side, nothing will happen, but the sharp head of needle will penetrate easily into the balloon. CNTs in their vertical mode will drop more easily into the gas bubbles and hence penetrate easily into them. This would probably be the reason of lower DPAs for VON layers. The sparks can diffuse CNTs toward the sample easier than HON layers, hence DPAs have lower average diameters.

On the other hand, according to the results presented in the previous sections, an evaluation of the proposed mechanism can be done here. The deposited material for each spark (and hence each DPA on the coating surface) is the volume of each DPA. As the coating thickness and also the DPA's diameter increase by the increase of processing time, so the height of each DPA can be assumed as a function of its size (its diameter for circular shapes). So the volume of each DPA is obtained as:

$$V_{DPA} = \pi \cdot (d_{DPA}/2)^2 \cdot (\alpha \cdot d_{DPA}) = \pi\alpha(d_{DPA})^3/4 \quad (1)$$

Where $\alpha.d_{DPA}$ is the height if DPA cylinder and $\alpha$ is a constant value. The deposited material over the whole surface of the cathode can be calculated as $N_{DPA}.V_{DPA}$ for one unit of the processing time. So the total layer has a volume ($V_T$) equal to $N_{DPA}.V_{DPA}.t$, in which t is the processing time. As indicated earlier, $d_{DPA}$ is approximately constant, so $V_{DPA}$ is also near a constant value. $N_{DPA}$ changes linearly with respect to $t^{-0.5}$. So $V_T$ is a function of $t^{0.5}$, which is in a good agreement with previous results [25].

$d_{DPA}$ is higher for HON layers and hence $V_T$ is also higher for HON at similar coating times. So the differences in Figure 2 (coating thickness) are also predictable by this mechanism. It is notable that the amount of CNTs did not affect the volume of deposited material. So the differences in the amount of CNTs in VON and HON layers can not be affected by those calculations. The porosity of both of these fabricated layers is considered to be similar. Roughness of VON layers is higher than that of HON layers. Lower $d_{DPA}$ means of more valley-like structures among these areas and thus higher values of surface roughness. On the other hand it seems that the gaps among the vertical CNTs are more efficient in this case.

## 5. Wear analysis

Figure 10 shows the results of wear test on both VON and HON layers. The friction coefficient decreased from 0.2 to 0.1 for the nanocomposite layer, while HON layers showed lower

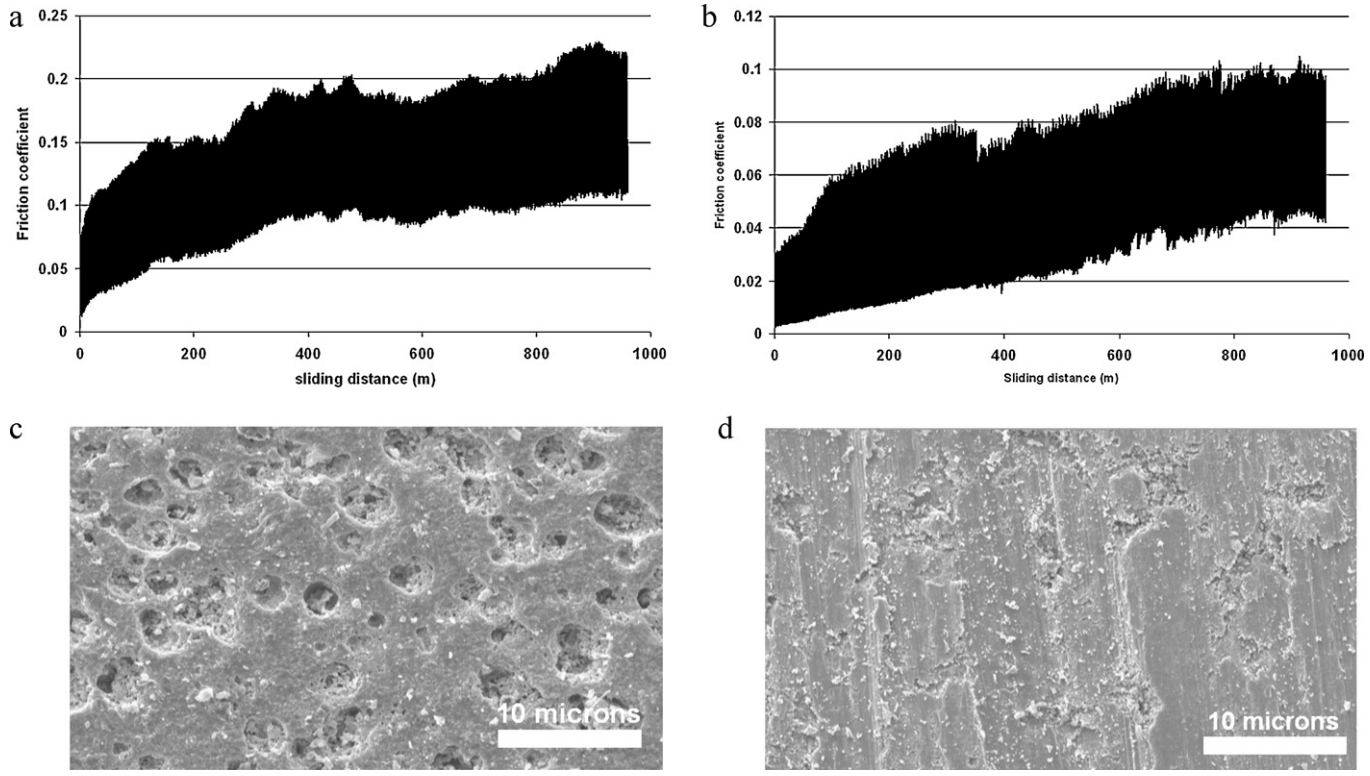


Figure 10. Friction coefficients and SEM microstructures of worn surfaces for (a, c) VON and (b, d) HON layers.

values than VON layers (Figure 10a). Study of worn surface revealed that in VON, partial zones of their surface were removed while the surface of HON was removed uniformly. The orientations of CNTs can affect the removal mechanism. As the sliding pin was moved parallel to the surface, the horizontal CNTs acted like nano-lubricants and removed slightly from the surface. But the vertically oriented CNTs were broken during the wear test due to their collision with the sliding pin from their side [43–45]. The necessary force to break the CNTs increases the friction coefficient due to more force necessary for removing the coating. The lowest wear rate of the fabricated layer ($5 \times 10^{-6}$ mm$^3$/Nm) decreased by near 400% for the nanocomposite coating with respect to the soft substrate and the VON layers showed higher wear rate than the HON layers. Partial removal of the coating is probably the reason of more wear rate of the VON layers than the HON layers.

## 6. Conclusions

1) Horizontal and vertical oriented nanocomposite layers were successfully fabricated by embedding carbon nanotubes in aluminum carbide based coating fabricated by plasma electrolysis. In order to fabricate these layers, a relatively high magnetic field was used to adjust the orientation of the layers.
2) The coating thickness was changed linearly with respect to the second root of the processing time. VON layers showed lower deposition rates than the HON fabricated layers. Also the roughness values of the VON layers were higher than those of the HON layers. Hardness values of the VON layers were a little more than that of the HON layers. Thicker layers have more ability for load bearing.
3) Embedding of carbon nanotubes decreased the average size of the aluminum carbide matrix. The microstructure of coating was composed of some similar deposited planar areas, which their average size for VON layers was lower than for HON layers. TEM nanostructures revealed that the distribution of CNTs is approximately similar in both VON and HON layers.
4) However the size of DPAs was different for the HON and VON layers but their size was not changed with increased time. Distribution of the DPAs was changed in terms of $t^{-0.5}$ with respect to the processing time.
5) The vertically oriented carbon nanotubes were embedded in gas bubbles more easily than the horizontally oriented ones. Evaluation for the volume of deposited material revealed that the proposed mechanism is valid for these coatings.
6) Wear tests showed that friction coefficient decreased in both fabricated layers with respect to raw $Al_4C_3$. It was decreased more for VON than HON. Microstructures of the worn surfaces showed that the VON layer was removed partially in some areas while HON removed uniformly. VON showed more necessary force for its removal due to more force needed for breaking vertically oriented CNTs. The wear rates decreased near 400% for nanocomposite coating with respect to the soft substrate while the VON layers showed higher wear rates than the HON layers.

## Acknowledgements

The authors are grateful to Dr. J.A. Curran from Cambridge University (also Keronite international company) for his helpful discussions during investigations about different aspects of plasma electrolysis.

## References

[1] M. Aliofkhazraei, A.S. Rouhaghdam, T. Shahrabi, Abrasive wear behavior of $Si_3N_4/TiO_2$ nanocomposite coatings fabricated by plasma electrolytic oxidation, Surf. Coat. Technol. 205 (2010) S41–S46.
[2] R. Arrabal, E. Matykina, F. Viejo, P. Skeldon, G.E. Thompson, M.C. Merino, AC plasma electrolytic oxidation of magnesium with zirconia nanoparticles, Appl. Surf. Sci. 254 (21) (2008) 6937–6942.
[3] E. Matykina, R. Arrabal, F. Monfort, P. Skeldon, G.E. Thompson, Incorporation of zirconia into coatings formed by DC plasma electrolytic oxidation of aluminium in nanoparticle suspensions, Appl. Surf. Sci. 255 (5, Part 2) (2008) 2830–2839.
[4] A.L. Yerokhin, X. Nie, A. Leyland, A. Matthews, S.J. Dowey, Plasma electrolysis for surface engineering, Surf. Coat. Technol. 122 (2–3) (1999) 73–93.
[5] N.S. Qu, D. Zhu, K.C. Chan, Fabrication of Ni-$CeO_2$ nanocomposite by electrodeposition, Scripta Mater. 54 (7) (2006) 1421–1425.
[6] F.-f. Xia, M.-h. Wu, F. Wang, Z.-y. Jia, A.-l. Wang, Nanocomposite Ni-TiN coatings prepared by ultrasonic electrodeposition, Current Appl. Phys 9 (1) (2009) 44–47.
[7] Y.-J. Xue, H.-B. Liu, M.-M. Lan, J.-S. Li, H. Li, Effect of different electrodeposition methods on oxidation resistance of Ni-$CeO_2$ nanocomposite coating, Surf. Coat. Technol. In Press, Corrected Proof.
[8] S. Komarneni, Nanocomposites, Journal of Materials Chemistry 2 (12) (1992) 1219–1230.
[9] J.U. Cho, J.-H. Wu, J.H. Min, J.H. Lee, H.-L. Liu, Y.K. Kim, Effect of field deposition and pore size on Co/Cu barcode nanowires by electrodeposition, J. Magnetism Magnetic Mater 310 (2 Part 3) (2007) 2420–2422.
[10] K.C. Chan, G.F. Wang, C.L. Wang, K.F. Zhang, Low temperature superplastic gas pressure forming of electrodeposited Ni/SiCp nanocomposites, Mater. Sci. Eng. A 404 (1–2) (2005) 108–116.
[11] R. Sen, S. Bhattacharya, S. Das, K. Das, Effect of surfactant on the co-electrodeposition of the nano-sized ceria particle in the nickel matrix, J. Alloy Compounds 489 (2) 650-658.
[12] S. Spanou, E.A. Pavlatou, N. Spyrellis, Ni/nano-TiO2 composite electrodeposits: Textural and structural modifications, Electrochim. Acta 54 (9) (2009) 2547–2555.
[13] J.N. Coleman, U. Khan, W.J. Blau, Y.K. Gun'ko, Small but strong: A review of the mechanical properties of carbon nanotube-polymer composites, Carbon 44 (9) (2006) 1624–1652.
[14] J.-P. Salvetat-Delmotte, A. Rubio, Mechanical properties of carbon nanotubes: a fiber digest for beginners, Carbon 40 (10) (2002) 1729–1734.
[15] P.G. Whitten, G.M. Spinks, G.G. Wallace, Mechanical properties of carbon nanotube paper in ionic liquid and aqueous electrolytes, Carbon 43 (9) (2005) 1891–1896.
[16] A. Chiolerio, S. Musso, M. Sangermano, M. Giorcelli, S. Bianco, M. Coïsson, A. Priola, P. Allia, A. Tagliaferro, Preparation of polymer-based composite with magnetic anisotropy by oriented carbon nanotube dispersion, Diamond Related Mater. 17 (7–10) (2008) 1590–1595.
[17] A.T.T. Koh, J. Hsieh, D.H.C. Chua, Structural characterization of dual-metal containing diamond-like carbon nanocomposite films by pulsed laser deposition, Diamond Related Mater. 19 (5–6) (2010) 637–642.
[18] A.R. Beaber, J. Hafiz, J.V.R. Heberlein, W.W. Gerberich, S.L. Girshick, Wear behavior in SiC-TiX multilayered nanocomposite coatings, Surf. Coat. Technol. 203 (5–7) (2008) 771–775.
[19] J.D. Pearson, M.A. Zikry, K.J. Wahl, Microstructural modeling of adaptive nanocomposite coatings for durability and wear, Wear 266 (9–10) (2009) 1003–1012.

[20] L. Shi, C. Sun, P. Gao, F. Zhou, W. Liu, Mechanical properties and wear and corrosion resistance of electrodeposited Ni-Co/SiC nanocomposite coating, Appl. Surf. Sci. 252 (10) (2006) 3591–3599.
[21] M. Aliofkhazraei, C. Morillo, R. Miresmaeili, A. Sabour Rouhaghdam, Carburizing of low-melting-point metals by pulsed nanocrystalline plasma electrolytic carburizing, Surf. Coat. Technol. 202 (22–23) (2008) 5493–5496.
[22] V. Dobrokhotov, C.A. Berven, Electronic transport properties of metallic CNTs in an axial magnetic field at nonzero temperatures: A model of an ultra-small digital magnetometer, Physica E: Low-dimensional System Nanostructures 31 (2) (2006) 111–116.
[23] A. Bensely, A. Prabhakaran, D. Mohan Lal, G. Nagarajan, Enhancing the wear resistance of case carburized steel (En 353) by cryogenic treatment, Cryogenics 45 (12) (2005) 747–754.
[24] J. Victoria-Hern?ndez, D. Hern?ndez-Silva, M. Vite-Torres, Microstructural characterization and sliding wear behavior of ultra high carbon steels processed by mechanical alloying, Wear 267 (1–4) (2009) 340–344.
[25] M. Aliofkhazraei, A. Sabour Roohaghdam, A novel method for preparing aluminum diffusion coating by nanocrystalline plasma electrolysis, Electrochem. Commun. 9 (11) (2007) 2686–2691.
[26] X.-M. Li, Y. Han, Porous nanocrystalline $Ti(C_xN_{1-x})$ thick films by plasma electrolytic carbonitriding, Electrochem. Commun. 8 (2) (2006) 267–272.
[27] Q. Luo, P.E. Hovsepian, D.B. Lewis, W.D. Münz, Y.N. Kok, J. Cockrem, M. Bolton, A. Farinotti, Tribological properties of unbalanced magnetron sputtered nano-scale multilayer coatings TiAlN/VN and TiAlCrYN deposited on plasma nitrided steels, Surf. Coat. Technol. 193 (1–3) (2005) 39–45.
[28] S.L. Nie, G.H. Huang, Y.P. Li, Tribological study on hydrostatic slipper bearing with annular orifice damper for water hydraulic axial piston motor, Tribology International 39 (11) (2006) 1342–1354.
[29] W. Xue, H.L. Hosick, A. Bandyopadhyay, S. Bose, C. Ding, K.D.K. Luk, K.M.C. Cheung, W.W. Lu, Preparation and cell-materials interactions of plasma sprayed strontium-containing hydroxyapatite coating, Surf. Coat. Technol. 201 (8) (2007) 4685–4693.
[30] M. Aliofkhazraei, A. Sabour Rouhaghdam, Fabrication of TiC/WC ultra hard nanocomposite layers by plasma electrolysis and study of its characteristics, Surf. Coat. Technol. 205 (2010) S51–S56.
[31] R.H.U. Khan, A.L. Yerokhin, T. Pilkington, A. Leyland, A. Matthews, Residual stresses in plasma electrolytic oxidation coatings on Al alloy produced by pulsed unipolar current, Surf. Coat. Technol. 200 (5–6) (2005) 1580–1586.
[32] K. Wang, B.H. Koo, C.G. Lee, Y.J. Kim, S. Lee, E. Byon, Effects of Hybrid Voltages on Oxide Formation on 6061 Al-alloys During Plasma Electrolytic Oxidation, Chinese J. Aeronautics 22 (5) (2009) 564–568.
[33] W. Xue, Q. Zhu, Q. Jin, M. Hua, Characterization of ceramic coatings fabricated on zirconium alloy by plasma electrolytic oxidation in silicate electrolyte, Mater. Chem. Phys. 120 (2–3) (2010) 656–660.
[34] Z. Yao, Y. Jiang, Z. Jiang, F. Wang, Z. Wu, Preparation and structure of ceramic coatings containing zirconium oxide on Ti alloy by plasma electrolytic oxidation, J. Mater. Process. Technol. 205 (1–3) (2008) 303–307.
[35] A.L. Yerokhin, A. Shatrov, V. Samsonov, P. Shashkov, A. Pilkington, A. Leyland, A. Matthews, Oxide ceramic coatings on aluminium alloys produced by a pulsed bipolar plasma electrolytic oxidation process, Surf. Coat. Technol. 199 (2–3) (2005) 150–157.
[36] P. Gupta, G. Tenhundfeld, E.O. Daigle, D. Ryabkov, Electrolytic plasma technology: Science and engineering–An overview, Surf. Coat. Technol. 201 (21) (2007) 8746–8760.
[37] X.-M. Li, Y. Han, Mechanical properties of Ti(C0.7N0.3) film produced by plasma electrolytic carbonitriding of Ti6Al4V alloy, Appl. Surf. Sci. 254 (20) (2008) 6350–6357.
[38] X.-M. Li, Y. Han, Y.-S. Li, Synthesis of nanocrystalline $Ti(C_xN_{1-x})$ thick films on titanium by plasma electrolytic carbonitriding, Surf. Coat. Technol. 201 (9–11) (2007) 5326–5329.
[39] D.L. Hitt, A. Prosperetti, Viscous forces on acoustically levitated gas bubbles, Nonlinear Analysis 63 (5–7) (2005) e1517–e1527.
[40] A.V. Nguyen, G.J. Jameson, Sliding of fine particles on the slip surface of rising gas bubbles: Resistance of liquid shear flows, Int. J. Multiphase Flow 31 (4) (2005) 492–513.
[41] F. Omota, A.C. Dimian, A. Bliek, Adhesion of solid particles to gas bubbles. Part 1: Modelling, Chem. Eng. Sci. 61 (2) (2006) 823–834.
[42] T. Tao, X.F. Peng, D.J. Lee, Force of a gas bubble on a foreign particle in front of a freezing interface, J. Colloid Interface Sci. 280 (2) (2004) 409–416.
[43] X.H. Chen, C.S. Chen, H.N. Xiao, H.B. Liu, L.P. Zhou, S.L. Li, G. Zhang, Dry friction and wear characteristics of nickel/carbon nanotube electroless composite deposits, Tribology Int. 39 (1) (2006) 22–28.
[44] I.-Y. Kim, J.-H. Lee, G.-S. Lee, S.-H. Baik, Y.-J. Kim, Y.-Z. Lee, Friction and wear characteristics of the carbon nanotube-aluminum composites with different manufacturing conditions, Wear 267 (1–4) (2009) 593–598.
[45] L.C. Zhang, I. Zarudi, K.Q. Xiao, Novel behaviour of friction and wear of epoxy composites reinforced by carbon nanotubes, Wear 261 (7–8) (2006) 806–811.